

HEAT TRANSFER AND FRICTION IN CIRCULAR DUCTS WITH SHAPED RIBS

L. Bonanni¹ - R. Da Soghe¹ - B. Facchini¹ - M. Micio¹ - M. Pievaroli¹ - L. Tarchi¹
L. Abba² - M. Maritano²

¹ Department of Energy Engineering, Università di Firenze, 50139, Via S. Marta 3, Firenze, Italy.
marco.pievaroli@htc.de.unifi.it; mirko.micio@htc.de.unifi.it

² Ansaldo Energia S.p.A., 16152, Via N. Lorenzi 8, Genova, Italy.

ABSTRACT

ElectroChemical Machining (ECM) is a conventional manufacture technology in drilling radial cooling channels within gas turbine blades. Coolant air flows inside these internal channels and passes through holes located at the blade leading and trailing edge. Generally ECM is used to manufacture cylindrical holes; nevertheless a specific kind of ECM, named Shaped Tube Electrolytic Machining (STEM) technique, allows to produce holes with variable diameter, that can be considered as tubes of circular cross section having a repeated-rib roughness.

Application of this kind of ribbed channels can improve heat transfer performance compared to cylindrical holes, without increasing manufacture costs.

This paper presents an experimental study concerning the heat transfer and friction factor characteristics of four ducts with shaped ribs for fully developed turbulent internal flows. The four circular ribbed ducts show two different pitch-to-rib height ratios ($p/e = 10 - 13.3$) and two different rib height-to-hydraulic diameter ratios ($e/D_h = 0.0714 - 0.0952$). Moreover the four models are classified by the rib shape, and named *Sharp* and *Smooth*.

Transient tests were performed varying the Reynolds number at the inlet section from 10000 to 40000. Heat transfer coefficients maps were evaluated using narrow band Thermo-chromic Liquid Crystals (TLC), while friction coefficients were calculated measuring pressure drop along the ducts with piezoresistive pressure sensors in cold tests.

Results report heat transfer coefficient profiles and pressure losses along the stream direction for all tested geometries as function of the Reynolds number. Heat transfer and friction coefficients are also compared to values for a smooth tube.

Moreover, for each geometry, the streamwise averaged Nusselt numbers have been fitted in order to highlight Reynolds number dependence ($Nu = A \cdot Re^B$).

A comparison with some published correlations for square and rectangular ribbed channels showed that using a correction factor it is possible to obtain the heat transfer coefficient for circular ribbed ducts.

Experimental results highlight that, keeping constant e/D , the *Smooth* geometry provide same global heat transfer performances with lower pressure losses than *Sharp* ones.

NOMENCLATURE

A	Passage area of the duct [m^2]	<u>Subscripts</u>	
c_p	Specific heat capacity [J/kgK]	a	Ambient air
C	Corrective term of heat transfer coefficient $[-]$	f	Inlet flow
d	Flat length between two ribs [mm]	$green$	Refers to green peak intensity of TLC
D	Duct hydraulic diameter [mm]	i	Wall initial condition
e	Rib height [mm]	w	Wall
f	Friction factor $[-]$	x	Axial streamwise direction
h	Heat transfer coefficient [W/m^2K]	0	Refers to smooth tube correlations
$\overline{h_e}$	Average heat transfer coefficient [W/m^2K]	<u>Acronyms</u>	
k	PMMA thermal conductivity [W/mK]	ECM	ElectroChemical Machining
L	Duct length [mm]	$PMMA$	Poly Methyl MethAcrylate
Nu	Nusselt number = hD/k_f $[-]$	$STEM$	Shaped Tube Electrolytic Machining
p	Pressure of air [Pa]	TIT	Turbine Inlet Temperature
P	Rib pitch [mm]	TLC	Thermocromic Liquid Crystals
Pr	Prandtl number $[-]$	<u>Greeks</u>	
Re	Flow Reynolds number = $\rho v D / \mu$ $[-]$	α	PMMA thermal diffusivity [m^2/s]
St	Stanton number = $Nu/RePr$ $[-]$	ρ	Air density [kg/m^3]
t	PMMA wall thickness [mm]	μ	Air viscosity [Ns/m^2]
t_v	TLC event time [s]		
T	Temperature of air [K]		
v	Inlet flow velocity in duct [m/s]		

INTRODUCTION

An improvement in overall efficiency and power output for both industrial and aeronautical gas turbines can be achieved increasing turbine inlet temperature (TIT) beyond melting points of components. An efficient cooling system is hence necessary to protect mechanical components from thermal stresses, assuring them a satisfactory lifetime.

Turbine vanes and blades usually employ a combination of external and internal cooling techniques such as internal convection, jet impingement and external film cooling. As regards internal cooling techniques, the rib turbulated cooling is one effective way to increase heat transfer coefficient within vanes and blades and to maintain metal temperature below critical limits.

The ribs, that are repeated along internal cooling channels, are typically cast on walls as projections from the internal surface into the flow. It is well known that ribs cause separation from the flow at the rib tops and reattachment to the flow between the ribs; this mechanism increases fluid turbulence and mixing among the fluid elements near the wall with the cooler ones in the middle of the flow-path. Therefore ribbed ducts provide two favourable contributions to enhance internal heat transfer: increase of turbulence level and increase of heat exchange area. On the other hand the presence of ribs induce a pressure drop along the channels. Consequently, designers have to find out the best rib geometry in order to obtain the highest heat transfer coefficients with the minimum friction penalty across the internal cooling passages. To reach this goal designers depend on experimental data and on semi-empirical correlations over a wide range of geometric parameters. These correlations primarily were derived from the law of the wall similarity for flow over rough surfaces; Nikuradse (1965) developed the so-called friction similarity law to correlate friction data for fully developed turbulent flows in tubes with a sand roughness, while Dipprey and Sabersky (1963) developed the so-called heat transfer similarity law to correlate heat transfer data for the same problem. Both similarity methods have been extended by Webb et al. (1971) to correlate both friction and heat transfer data for turbulent flows in rib-roughened tubes. Since the study of Webb et al. was performed on fully ribbed circular pipes, similar to those of the present work, it has been assumed as an important reference point in the

present work.

Moreover, starting from the wall similarity laws discussed earlier, J.C. Han has made a large amount of research in this area and has developed semi-empirical correlations, which are still today important reference tools in the design of turbine blade cooling passages. In his earlier work Han et al. (1985) developed correlations for the average friction factor and the average heat transfer coefficient for flows in square ducts with two and four ribbed walls. These correlations include the effect of rib angle of attack, pitch-to-rib height ratio and Reynolds number on the pressure drop and the average heat transfer coefficients. In later works Han and Park (1988) extended the previous correlations to rectangular channels with two and four ribbed walls and covered a higher range of validity in terms of channel aspect ratio, rib spacing, rib height and Reynolds number.

In the present work the foregoing literature correlations have been used as tools of reference in the predicting of heat transfer enhancement and pressure penalty of four ribbed ducts for a their potential application as radial cooling channels in gas turbines. A specific technique of electro-chemical machining, named Shaped Tube Electrolytic Machining (STEM), allows to manufacture this kind of ribbed ducts by using a shaped electrode. During STEM process the electric field intensity of the electrode is varied so as to realize variable diameter holes.

With regard to experimental investigation transient surface temperature techniques can be applied to determine local and average heat transfer coefficient distributions in ribbed ducts. Recently Amro et al. (2007) applied transient liquid crystal method to measure the heat transfer coefficient in internal cooling channels using optically transparent models. This same technique was applied in the present investigation.

The present experimental work aims to investigate the effect of pitch-to-rib height ratio, rib height-to-hydraulic diameter ratio and rib shape on the pressure losses and heat transfer performances for inlet Reynolds number varied from 10000 to 40000. Since no many studies have been reported on circular cooling ducts the present data have been compared with the aforesaid literature correlations for square and rectangular ribbed channels. From this comparison correction factors for both pressure losses and heat transfer coefficients have been obtained so as to apply Han's correlations to the present circular ribbed channels.

EXPERIMENTAL FACILITY

The experimental survey was performed at the Dipartimento di Energetica "S. Stecco" of the Università degli Studi di Firenze. A test facility was designed to measure local and average heat transfer coefficients and overall pressure drop across four different circular ribbed ducts and one circular smooth duct. The four ribbed geometries are characterized by the following geometric parameters: duct diameter D , rib height e , streamwise rib pitch P_x and rib shape (*Sharp*, *Smooth*). The *Sharp* shape reproduces the ideal target of STEM machining, while the *Smooth* shape reproduces a more realistic machining. The duct diameter D is that measured at the base of the ribs.

The four geometries are characterized by the same values of hydraulic diameter D and rib pitch P_x but two different values of rib height e ; as shown in the table of Figure 1, this results in two different pitch-to-rib height ratios ($P_x/e = 10 - 13.3$), two different rib height-to-hydraulic diameter ratios ($e/D = 0.0714 - 0.0952$), two different rib shapes and a constant rib pitch-to-hydraulic diameter ratio ($P_x/D = 0.952$). Figure 1 also shows a schematic drawing of the ducts layout; in this example geometries have the same P_x/e and e/D values but a different rib shape.

The test rig, as depicted in the scheme of Figure 2, consists of an open-loop suction type wind tunnel which allows the complete control of the air mass flow rate and air inlet temperature. A flow rate of air is supplied to the test section by two rotary vane vacuum pumps with a total capacity of $600 \text{ m}^3/\text{h}$, and metered through a calibrated nozzle. The air flow rate is set up by guiding the pump

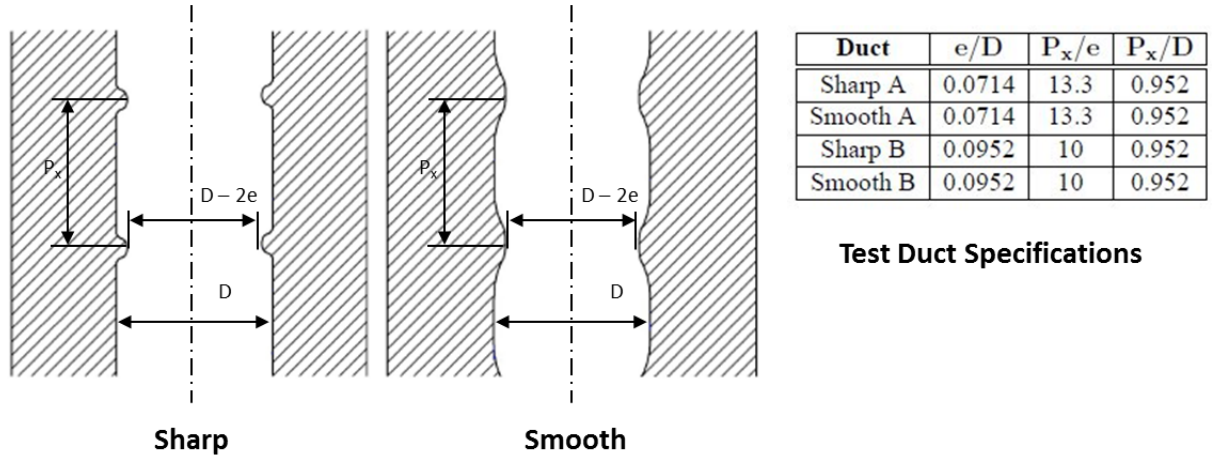


Figure 1: Drawings of *Sharp* and *Smooth* ribbed ducts with test duct geometry specifications

speeds and using a throttle valve located between the vacuum pumps and the test section.

The air enters in the test rig through the calibrated nozzle, then passes through a 16 kW electronically controlled electric heater before entering the test model. Flow is developed in a smooth section of insulated rubber tubing located between the heater and the test section. Inside this section the flow crosses a honeycomb and two screens, which allow to set an uniform velocity profile at the inlet of the test model. Each test model is attached to the test rig by two tapered connections.

A pressure scanner Scanivalve DSA 3217, with temperature compensated piezoresistive relative pressure sensors, measures the pressure in 5 different locations, along the ribbed walls, with a maximum accuracy of 6.9 Pa; these permit to measure static pressure drop in the test ducts.

Three T type thermocouples connected to a data acquisition/data switch unit (Agilent 34970A) measure the following temperatures: ambient air T_a , inlet flow T_f and duct wall initial temperature T_i .

Heat transfer coefficient is measured by a transient technique; surface temperature T_w has been evaluated by means of narrow band Thermochromic Liquid Crystals (TLC) supplied by Hallcrest LCR and active from 40°C to 41°C. TLCs have been calibrated following the steady state gradient method (Chan et al. (2001)); the green color peak intensity was found at 40.2°C and it was used as event temperature T_{green} in the data reduction procedure.

A digital camera (Sony SX90CR) records a sequence of color bitmap images (1248 x 48 pixel) at the rate of 13 frames per second from the TLC painted surface on a PC (IEEE-1394 standard). A preliminary analysis has been conducted to assess the optimal value of camcorder frame rate; the value of 13 fps has been chosen to ensure a good accuracy in the estimate of liquid crystals event time without excessively increasing images post-processing time.

The illuminating system consists in a 8 W white led array of 750-800 lumen to be able to ensure an uniform illumination on the test surface.

The test articles are completely made of transparent PMMA (Poly Methyl MethAcrylate - thermal conductivity $k = 0.19 W/mK$) allowing the required optical access for TLC measurements. The low thermal conductivity of PMMA and the specific wall thickness of the test articles (about 15 mm) minimize the penetration depth of the heat during the test. This allows to satisfy criteria for semi-infinite modeling, as reported by G.Wagner et al. (2005); in fact at lower Reynolds numbers the experimental transient times are always lower than times required by the heat to reach the external surface of the test article. This ensures quasi-adiabatic conditions during the tests.

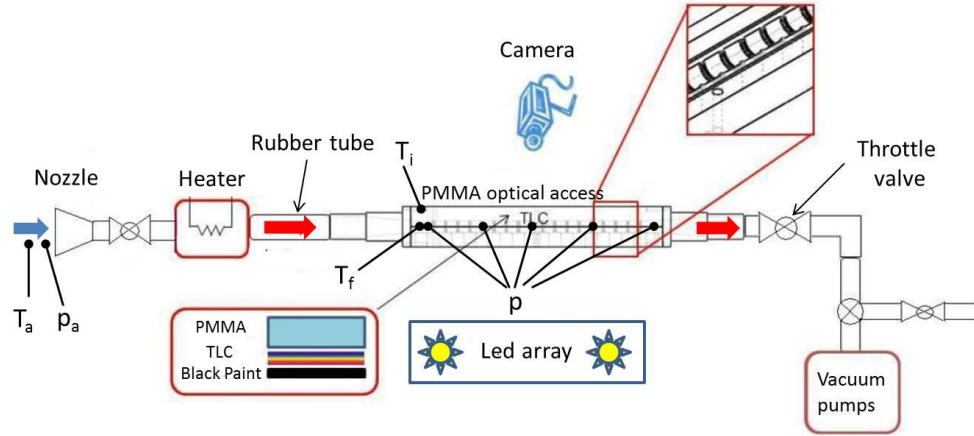


Figure 2: Test rig scheme

EXPERIMENTAL PROCEDURE AND METHOD

First of all each geometry was investigated in cold flow conditions to evaluate friction factor and pressure losses varying the Reynolds numbers in the inlet section from 10000 to 40000 with six steps equal to 5000. In cold tests the pressure drop across the different ducts was measured by piezoresistive relative pressure sensors. In a fully developed duct flow, the Fanning friction factor definition was used to calculate the f coefficient from the pressure drop across the flow channel, the velocity and the density of the air:

$$f = 0.5 \left(\frac{D}{L} \right) \left(\frac{\Delta p}{\rho v^2} \right) \quad (1)$$

Then heat transfer tests were performed in the same Reynolds number range of the cold tests, but preheating the flow before the start of each test. Local heat transfer coefficients are evaluated using a transient technique; in this way it is possible to monitor the temporal evolution of the surface temperature in conjunction with the solution of a transient heat conduction model penetrating to the wall substrate. During the test, the air is first heated using the electric heater to a desired temperature within the TLC response range. When the air temperature reaches $50 - 70^\circ C$ in the heater, which also acts as plenum chamber, the throttle valve is suddenly switched allowing the air passage through the test model. In this way it is possible to realize a step change in the fluid temperature T_f relative to uniform initial model temperature. Simultaneously with the switching of the valve, temperature and pressure information are recorded in separate files into the PC, and camcorder starts recording frames. Test stops when all points of the measurement surface have passed through the green color peak intensity. The minimum time to reach the TLC green peak intensity (TLC event time) was from 10 s to 55 s after the switching of the valve, while the time duration of the tests was between 100 s to 230 s, depending on Reynolds number and inlet flow temperature T_f . The camera records a maximum number of digital images varying from 1300 to 3000 depending on the flow conditions of each test. The usual way of calculating a detailed heat transfer coefficient distribution for the transient experiments is based on the transient heating, assuming one-dimensional conduction in a semi-infinite plate (Ireland et al. (1993), Camci (1995)). This is the solution of the one-dimensional Fourier equation for the case of an infinitely thick plate, initially at a uniform temperature T_i , exposed to a step change in the temperature of the fluid T_f . As reported by Maiuolo et al. (2012) it is more reliable to apply an explicit finite-difference method in cylindrical coordinate in order to solve one-dimensional transient conduction across model thickness taking surface curvature effect into account. Therefore

in the present work a such method has been applied solving the following equation in cylindrical coordinates:

$$\rho c_p \frac{\partial T}{\partial t} = \frac{k}{r} \frac{\partial}{\partial r} \left(r \frac{\partial T}{\partial r} \right) \quad (2)$$

The local time-dependent wall temperature T_w is measured by detecting TLC green peak, while initial wall temperature T_i and flow temperature T_f are measured by two thermocouples respectively located on the PMMA external surface and at the inlet section of the test duct. The unknown heat transfer coefficient h is determined through an iterative procedure, using the previous temperature information together values of PMMA thermal diffusivity α and thermal conductivity k and TLC event time t_v . The latter value is determined as difference between the start time of the test and the time required to reach TLC green peak at any location of the test surface.

Moreover since a perfect step change of temperature cannot be realized, a principle of superposition was applied to model flow temperature profile $T_f(t)$ in data reduction procedure.

Experimental data post-process

The post-process of each experimental data session was divided into three main stages. First of all, the acquired digital images were analysed using a Matlab[®] routine in order to relate each pixel of the test area with its own event time t_v . As a result of this procedure a matrix with the same dimensions of the analysed area was obtained. Figure 3 shows an example of a digital image acquired during a transient test for $T_f = 62.5^\circ C$ and $Re=40000$ after 30 s from the beginning of the test .

During the tests a gradual and uniform TLC color response was observed in the streamwise direction, with the exception of the closest part to the inlet section of the duct. Since this latter part took a long time to reach the green color peak, it was established to exclude it from the post-processing stages.

Moreover to eliminate problems with the viewing angle of the surface curvature, only the area close to the center axial line of the digital image was analyzed; in fact, as reported in Figure 3, only the pixels within the white rectangle have been taken into account in the post-process.

In the second stage the above-mentioned matrix was employed as input data of a Fortran code; using the explicit finite-difference method, the heat equation was solved along model thickness and local heat transfer coefficients were obtained from TLC event times matrix.

In the final stage of post-processing a correction procedure was applied to the local heat transfer coefficients; in fact these coefficients have its reference temperature based on the inlet temperature of the test rig, rather than the local bulk mean temperature. Since flow temperature decreases downstream the channel, especially in flow channels with large length to diameter ratio, the heat transfer coefficient based on the inlet temperature presents difficulty in data interpretation. To take this fact into account a method based on principle of energy balance was used to correct the local heat transfer coefficient. This method, presented by Chyu et al. (1998), can be summarized with the introduction of a corrective term as a function of the streamwise direction x :

$$C(x) = \frac{\frac{\rho c_p v}{h_e} \frac{A}{P_x}}{\frac{\rho c_p v}{h_e} \frac{A}{P_x} - 1} \quad (3)$$

where the term $\rho c_p v / \overline{h_e}$ is the reciprocal of the Stanton number while A/P_x is an area factor. Therefore the corrected heat transfer coefficient is calculated as product of C with the previous h coefficient.

Experimental uncertainty

The uncertainty analysis was performed following the standard ASME (1985) based on method proposed by Kline and McClintock (1953). Considering that the temperature accuracy is $\pm 0.5 K$,



Figure 3: **Example of TLC digital image acquired at $Re=40000$ and $t=30$ s**

differential pressure is $\pm 6.9 Pa$ and mass flow rate is $\pm 2 - 3\%$, the estimated uncertainty in evaluating the friction factor was below 10%. As regards the heat transfer coefficient, the highest uncertainty was about 13% and it was found at lower response times (i.e. higher HTC values).

EXPERIMENTAL RESULTS

Experimental results for ribbed ducts: Friction

As explained in the experimental procedure friction factors and pressure losses were evaluated in cold tests. Figure 4 shows the friction factors for all geometries and for all tested conditions. For comparison, the smooth tube correlation of Blasius is also reported as $f = 0.046Re^{-0.2}$.

As expected friction factor is greatest for the higher rib height-to-hydraulic diameter ratio cases of $e/D = 0.0952$ (*Sharp B* and *Smooth B*). Moreover, for the same e/D value, both A and B geometry with *Sharp* rib shape show higher friction factors than the *Smooth* ones respectively of 30% and 50%.

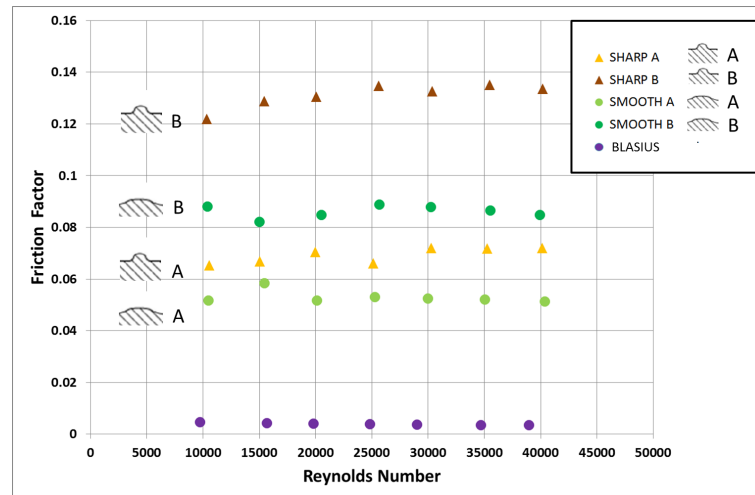


Figure 4: **Experimental results - friction factors for all tested geometries**

Experimental results for ribbed ducts: Heat Transfer

The convective heat transfer coefficient is measured along the streamwise direction using the data provided by the selected area on each digital image (Figure 3). Figures 5a and 5b show the characteristic behavior of a ribbed channel with a periodic heat transfer coefficient distribution for A geometries. Results for B geometries are similar but with higher peaks as a consequence of the higher e/D ratio. In all cases the higher peaks of heat transfer coefficient are obtained at the leading edge of each rib, then a separation occurs downstream each rib and the flow reattachment determines another peak of h coefficient between two consecutive ribs.

As expected, the heat transfer results indicate that the mean heat transfer coefficient increases with increasing Reynolds number. Moreover, although there is an analogy in the behavior of the two different rib shape, the *Sharp* geometries present higher peaks than the *Smooth* ones.

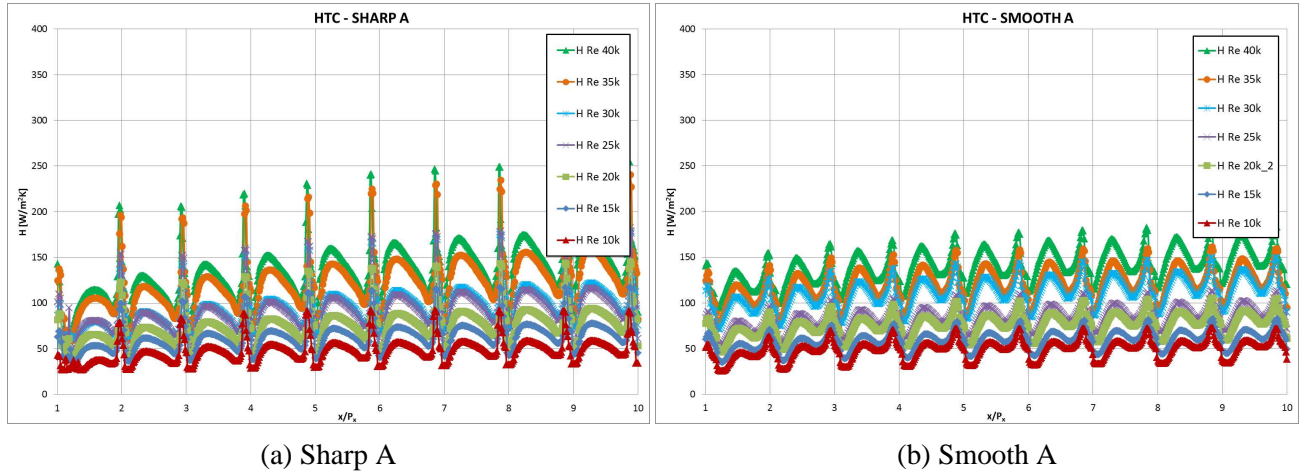


Figure 5: Experimental results - heat transfer coefficients along streamwise direction

Experimental heat transfer relationships

To summarize heat transfer results and find out reliable information for the manufacturer, averaged results in streamwise direction were calculated for all tested channels and an average Nusselt number was obtained for each Reynolds number. Then the streamwise averaged Nusselt numbers have been fitted as $Nu = ARe^B$, in order to highlight Reynolds number dependence for each ribbed geometry. Figure 6 resumes the duct test results of average Nusselt number as a function of Reynolds number for the four investigated geometries and for a smooth duct without ribs. The experimental results for this smooth duct show a good agreement with the smooth tube and fully developed turbulent flow Colburn correlation ($Nu = 0.023Re^{0.8}Pr^{0.33}$) within the experimental Re range and reach a maximum deviation of 10% at Re=40000.

With regard to ribbed geometries the experimental trends highlight an increase in the slope of the curve corresponding to the increase of rib height-to-hydraulic diameter ratio from 0.0714 to 0.0952. Moreover it is clear that, as regards A geometries, the rib shape does not affect the global heat transfer performance, while this same effect is more relevant for B geometries at the higher Reynolds numbers. Table 1 gives a summary of the four Nu-Re relationships found by experimental data. This table gives also the heat transfer enhancement factors Nu/Nu_0 for the four ribbed geometries; these values have been calculated forcing the best curves fitting to $Re^{0.8}$ and normalizing to the corresponding Nu_0 evaluated by the Colburn correlation provided above.

Duct	$Nu-Re$ relationship	Nu/Nu_0
Sharp A	$Nu = 0.0485Re^{0.755}$	1.62
Smooth A	$Nu = 0.0275Re^{0.809}$	1.60
Sharp B	$Nu = 0.0275Re^{0.823}$	1.86
Smooth B	$Nu = 0.01195Re^{0.853}$	1.74

Table 1: Experimental heat transfer relationships

Thermal-Friction performance comparison

Enhancement factors for friction and heat transfer were calculated, using smooth tube data (f_0 , St_0) of Blasius and Colburn correlations respectively as normalizing factors of Stanton numbers St and friction factors f obtained from experimental measurements. Figure 7a depicts the normalized Stanton number (St/St_0) against normalized friction factor (f/f_0). It is shown that, for each e/D

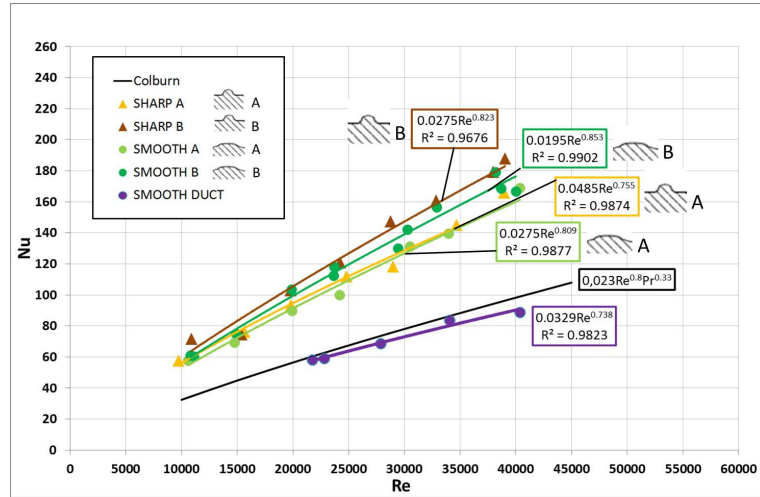


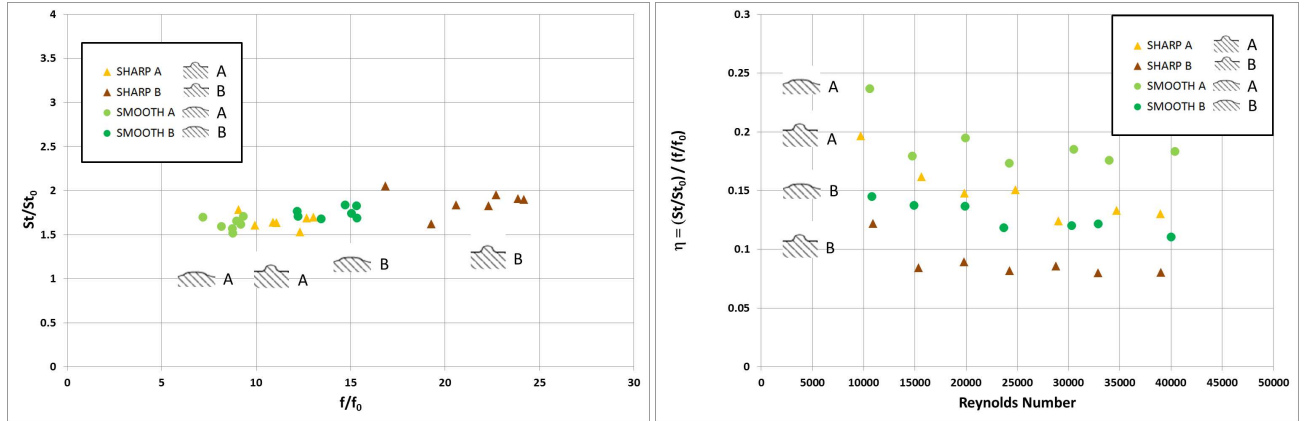
Figure 6: Nu-Re relationships for all ribbed geometries

ratio, the *Smooth* geometries offer a quite similar global heat transfer performance to *Sharp* ones with reduced friction losses.

To obtain a global performance factor for each flow condition an efficiency index was calculated as follows:

$$\eta = \frac{St/St_0}{f/f_0} \quad (4)$$

This efficiency index η versus Reynolds number Re is plotted in Figure 7b. These results suggest that the *Smooth A* geometry ensures the best efficiency on the whole Re range.



(a) Heat transfer and friction enhancement factors

(b) Efficiency index against Reynolds number

Figure 7: Thermal-Friction performance comparison for all tested geometries

COMPARISON WITH EXISTING CORRELATIONS

Correlations from three important well-known studies about rib turbulated cooling were used as a comparison term for the present experimental data, in order to find out if an existing correlation could be directly applied to the investigated geometries.

Table 2 gives a summary of the literature correlations used for this comparison and gives an overview of the different ranges of the these correlations together with the ranges of the present geometries.

Correlation	Case	Geometry	Re[x 10 ³]	α	e/D	P _x /e
Han 1985	Case 1	Square channel 2 rib walls	8 - 80	0°-90°	0.021-0.063	10-20
	Case 2	Square channel 4 rib walls	8 - 80	0°-90°	0.021-0.063	10-20
Han 1988	Case 3	Rectangular channel 2 rib walls	8 - 80	30°-90°	0.047-0.078	10-20
	Case 4	Rectangular channel 4 rib walls	8 - 80	30°-90°	0.047-0.078	10-20
Webb 1970	Case 5	Ribbed circular pipes	5 - 100	90°	0.01-0.04	10-40
Present Data		Ribbed circular pipes	10 - 40	90°	0.0714-0.0952	10-13.3

Table 2: Cases used as correlations of comparison

This table shows that some of the present e/D values fall just outside of the ranges investigated by Han and Webb.

Since the five different correlations does not allow to account for the two present rib shapes, each correlation can provide a single trend as a function of e/D and P_x/e , while data for *Sharp* and *Smooth* geometries have been grouped into the same comparison. With regard to friction factor comparisons, a good agreement is reached between Han's correlation for rectangular channel with four-sided ribbed walls (case 4) and present data, except for the *Sharp B* geometry. In fact for *Sharp A*, *Smooth A* and *Smooth B* geometries, the correlation shows relative deviations from 0.8% to a maximum of 16%, while concerning the *Sharp B* case the deviation reaches a maximum gap of 33%. When it comes to the heat transfer comparisons, all test cases are fitted very well by Han's correlation for square channels with two opposite ribbed walls (case 1); in all cases the relative deviation, in terms of Stanton number, falls within the range 2 – 10%.

DEFINITION OF A CORRECTION FACTOR FOR CIRCULAR RIBBED CHANNELS

As explained in the previous section, the Han's correlation for square channel with 2 ribbed walls (named in this section case1) is able to estimate with a good agreement present experimental results in terms of Stanton number. For this reason, in this section will be defined a correction factor for heat transfer and one for pressure losses which allows to use the Han's correlation for present geometries. The correction factor for heat transfer is defined as:

$$n = \frac{St_{exp}}{St_{case1}} \quad (5)$$

Figure 8a shows that the correction factor for Stanton number is very similar for all investigated geometries . It takes values close to 1 with a slight dependence by Reynolds number. Thus this factor takes form of:

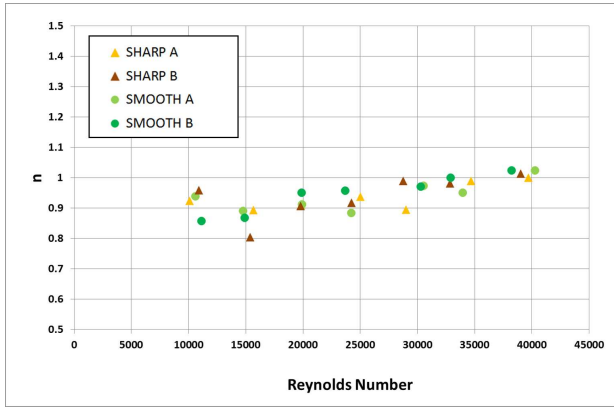
$$n = k_1 \cdot Re^{k_2} \quad (6)$$

Even if the correlation that shows the better agreement with present experimental results for pressure losses is the Han's correlation for rectangular channel with 4 ribbed walls (named in the previous section case 4), the correction factor was defined for correlation case 1. This is due to the fact that this correlation shows the better prediction capability for heat transfer point of view.

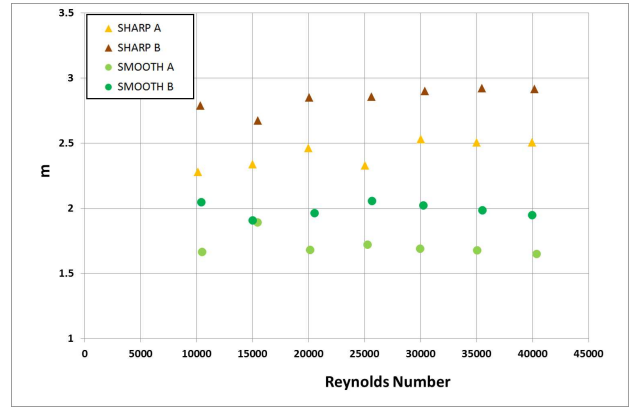
In figure 8b the correction factor for the friction factor for different Reynolds number is plotted for all investigated geometries. The correction factor is defined as:

$$m = \frac{f_{exp}}{f_{case1}} \quad (7)$$

Figure 8b points out that the correction factor for friction factor is almost independent from Reynolds number for each geometry while a strong dependence by geometric parameters is shown.



(a) Stanton number



(b) Friction factor

Figure 8: **Variation of correction factors with Reynolds number for all investigated geometries**

In order to correlate this dependence the geometry has been schematized using the geometric parameters showed in Figure 9. In particular, to distinguish the configuration shape from that smooth a new parameter d needs to be defined. This parameter is equal to the flat length between two ribs.

Using a linear interpolation of the parameter d/P_x , the configuration A and B have been correlated separately as shown in Figure 10a. Both equations have the same angular coefficient with a different offset. Thus the offset is correlated in order to take into account if configuration A or B is analyzed as a function of the parameter e/D . Finally the correction factor for friction factor (Figure 10b) takes the form of:

$$m = k_3 \cdot \frac{d}{P_x} + k_4 \cdot \frac{e}{D} + k_5 \quad (8)$$

Using these equations to evaluate the correction factor for Stanton number and friction factor, the error between experimental results and the calculated values is lower than 5% which is below the experimental accuracy.

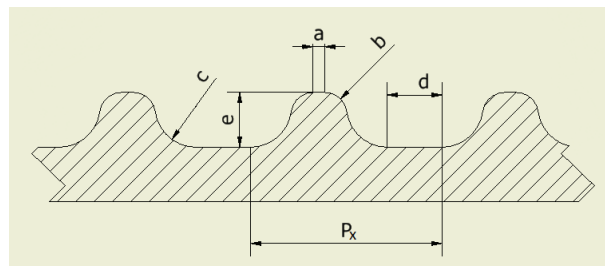


Figure 9: **Schematization of ribbed surface geometry**

CONCLUSIONS

An experimental investigation was performed on friction and heat transfer performance of four circular ribbed ducts. Friction factors and heat transfer coefficients measurements have been obtained for fully developed turbulent internal flows in circular tubes with two different pitch-to-rib height ratios ($P_x/e = 10-13.3$), two different rib height-to-hydraulic diameter ratios ($e/D = 0.0714-0.0952$) and two different rib shapes but with a constant rib pitch-to-hydraulic diameter ratio ($P_x/D = 0.952$). Both friction and heat transfer tests were performed varying Reynolds number at the inlet section from 10000 to 40000. Concerning the pressure losses evaluation, the experimental results show that

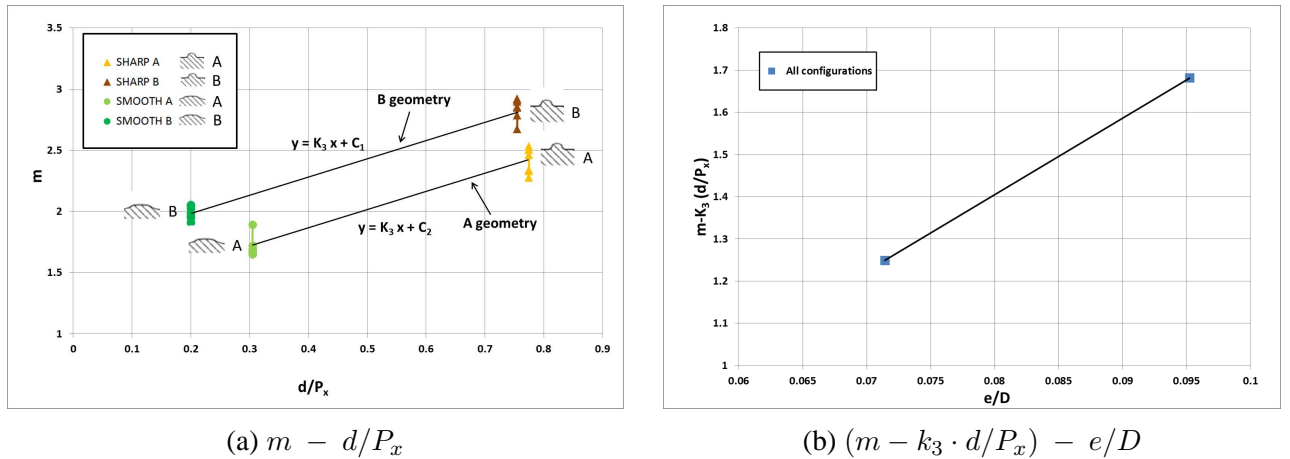


Figure 10: **Variation of correction factor for friction factor with geometric parameters for all investigated geometries**

the *Sharp* geometries reach friction factors higher than 30% compared to the *Smooth* ones. Moving on to the heat transfer results, the relationships between averaged Nusselt numbers and Reynolds numbers show an increase in the slope of the curve $Nu = ARe^B$ increasing the rib height. Moreover it is shown that the shape of the rib changes the height of the peaks in the local heat transfer coefficient distribution along streamwise direction but it does not affect the global heat transfer behavior.

The thermal and friction performance comparison, in terms of heat transfer and friction enhancement as a function of Reynolds number, confirms that the *Smooth* geometries have the same global heat transfer performance of the *Sharp* ones with reduced friction losses.

Moreover a comparison between experimental data and well-known correlations on rib turbulated cooling was performed; friction data are well fitted using the Han's correlation for rectangular channels with four-sided ribbed walls, while, concerning the heat transfer data, there is a good agreement with the Han's correlation for square channels with two opposite ribbed walls.

A correction factor for heat transfer coefficient has been defined as a function of Reynolds number for this correlation. This factor is close to 1 for high values and it decreases with decreasing Reynolds number. For Han's correlation for square channels with two opposite ribbed walls, a correction factor for friction factor has been defined in order to allow a correct estimation of pressure losses too. In this case, the geometric parameters are more important than Reynolds number. Thus this correction factor is a function of the ratio between the height of rib compared with the hydraulic diameter and the ratio of the length of the flat section with the pitch. With these correction factors the discrepancies with experimental results are less than 5%.

REFERENCES

- M. Amro, B. Weiganda, R. Poser, and M. Schnieder. An experimental investigation of the heat transfer in a ribbed triangular cooling channel. *International Journal of Thermal Sciences*, 46:491–500, 2007.
- ASME. Measurement uncertainty. In *Instrument and Apparatus*, volume ANSI/ASME PTC 19.1-1985 of *Performance Test Code*. ASME, 1985.
- C. Camci. Liquid crystal thermography. In *Temperature measurements*, Lecture Series 1996-07. von Karman Institute for Fluid Dynamics, 1995.
- T. L. Chan, S. Ashforth-Frost, and K. Jambunathan. Calibrating for viewing angle effect during heat transfer measurements on a curved surface. *International Journal of Heat and Mass transfer*, 44:2209–2223, 2001.
- M. K. Chyu, Y. C. Hsing, T. I. P. Shih, and V. Natarajan. Heat transfer contributions of pins and endwall in

- pin-fin arrays: effects of thermal boundary condition modelling. *ASME Turbo Expo*, (98-GT-175), 1998.
- D. F. Dipprey and R. H. Sabersky. Heat and momentum transfer in smooth and rough tubes at various prandtl numbers. *International Journal of Heat and Mass Transfer*, 6:329–353, 1963.
- G. Wagner, M. Kotulla, P. Ott, B. Weigand, and J. von Wolfersdorf. *Journal of Turbomachinery*, 127:175–182, 2005.
- J. C. Han and J. S. Park. Developing heat transfer in rectangular channels with rib turbulators. *International Journal of Heat and Mass Transfer*, 31:183–195, 1988.
- J. C. Han, J. S. Park, and C. K. Lei. Heat transfer enhancement in channels with turbulence promoters. *ASME Journal of Engineering for Gas Turbines and Power*, 107:628–635, 1985.
- P. T. Ireland, Z. Wang, and T. V. Jones. Liquid crystal heat transfer measurements. In *Measurements techniques*, Lecture Series 1993-05. von Karman Institute for Fluid Dynamics, 1993.
- S. J. Kline and F. A. McClintock. Describing uncertainties in single sample experiments. *Mechanical Engineering*, 75:3–8, 1953.
- F. Maiuolo, L. Andrei, C. Carcasci, R. Da Soghe, B. Facchini, L. Tarchi, and S. Zecchi. Heat transfer measurements in a leading edge geometry with racetrack holes and film cooling extraction. *ASME Turbo Expo*, (GT2012-69581), 2012.
- J. Nikuradse. Laws of flow in rough pipes. *VDI Forsch. 361 (1933). English Translation*, (NACA TM-1292), 1965.
- R. L. Webb, E. R. G. Eckert, and R. J. Goldstein. Heat transfer and friction in tubes with repeated-rib roughness. *International Journal of Heat and Mass Transfer*, 14:601–617, 1971.